

Spatial tidal asymmetry of Cochin estuary, West Coast, India

J. Vinita¹ · A. Shivaprasad¹ · N. T. Manoj^{2,3} · C. Revichandran¹ ·
K. R. Naveenkumar¹ · V. K. Jineesh¹

Received: 11 March 2015 / Accepted: 15 July 2015 / Published online: 6 August 2015
© Springer Science+Business Media Dordrecht 2015

Abstract An intensive one-month long observational campaign of tides and currents during dry season were used to describe the tidal dynamics and the spatial evolution of tidal asymmetry in Cochin estuary. The estuary is described as hyposynchronous since tidal amplitude and currents get attenuated towards upstream through frictional dissipation. The results showed that the tidal momentum balance along the main axis of the channel was dominated by pressure gradient and friction. The influence of advection was prevalent near the inlets and friction was greatest in the shallow upstream regions. Higher harmonics were generated in the estuary through nonlinear friction and advection causing tidal distortions. Being a mixed predominantly semidiurnal tidal regime, tidal asymmetry was quantified in terms of sample skewness to examine the spatial evolution in the total asymmetry. The principal astronomical tides (M₂, K₁ and O₁) interacted to engender flood dominance at the inlets. The compound tides and overtides generated inside the estuary were found to either augment or transform the asymmetry imposed by the principal tides. The study showed that friction causes flood dominance at the northern inlet (Munambam) and in the shallow regions of the upstream during dry season. In striking contrast, the Cochin inlet and the adjacent harbor area turned to be ebb-

dominant. These findings have implications for management and sediment transport mechanisms within the estuary.

Keywords Tidal asymmetry · Mixed semi-diurnal · Harmonic analysis · Friction · Skewness · Cochin estuary

Introduction

Tidal propagation in estuaries is affected by friction, river runoff, changes in bathymetry and the morphology of the channels which causes tidal asymmetry. The physical mechanisms responsible for these tidal distortions are represented by non-linear terms associated with friction, advection and conservation of mass (Parker 1991; Gallo and Vinzon 2005) and are manifested by the growth of higher harmonics within the system. The tidal asymmetry, while serving as an important mechanism of sediment transport (Dronkers 1986; Blanton et al. 2002), exerts effects on both the geological evolution of shallow estuaries and the navigability of estuarine channels (Speer and Aubrey 1985).

Cochin estuary, a tropical monsoonal estuary, is the second largest estuarine system situated on the west coast of India. Geomorphologically, it is classified as a bar-built estuary and therefore sometimes called as a “lagoon” (Rao and Balasubramanian 1996). For the establishment of Cochin port in 1936, the natural bar has been dredged out and the channel is now constantly maintained at 14 m draft by maintenance dredging to make the basin accessible for ocean going vessels (Strikwerda 2004). These human interventions such as navigation channel dredging, sand dredging and land reclamation have resulted in substantial alterations of the landscape of the system (Kumar et al. 2013). Hence, detailed investigations are required to evaluate the hydrodynamic response of the estuary to changes on geometry in order to assess the long term

✉ J. Vinita
jvinita@gmail.com

¹ CSIR-National Institute of Oceanography, Regional Centre, Dr. Salim Ali Road, P.B.No.16161, Kochi, Kerala, India 682 018

² CSIR-National Institute of Oceanography, Dona Paula, Goa 403004, India

³ Present address: General Commission for Survey (Govt. of Saudi Arabia), Riyadh, Saudi Arabia

impacts on the ecosystem. Unlike other estuaries of west coast of India, in Cochin estuary the tides are forced from two inlets and the estuarine morphology is complex with many interconnected channels and rivers. Therefore, studies on the tidal hydrodynamics of other Indian estuaries (Unnikrishnan et al. 1997; Manoj et al. 2009), while serving as a useful comparison, are not pertinent to Cochin estuary. Although several previous studies describe the tidal propagation in Cochin estuary (Srinivas et al. 2003a, b; Balachandran et al. 2008; Revichandran et al. 2011), the characteristics of tidal asymmetry have not been reported to date.

Tidal asymmetries in estuaries with mixed tides arise from the interaction of astronomical diurnal constituents (K1 and O1) and semidiurnal constituents (M2) (Hoitink et al. 2003). Nonlinear distortion within the system either counteracts or reinforces this incident asymmetry (Nidzicko 2010). Tides in Cochin estuary are mixed predominantly semidiurnal in nature. Hence, it is worthwhile to delineate the spatial evolution of tidal asymmetry, comparing the asymmetry arising from the interaction of the astronomical tides and the nonlinearities generated within the system. In this context, the primary objective of this paper is to precisely investigate the tidal hydrodynamics of Cochin estuary with special emphasis on the spatial evolution of tidal asymmetry. The paper is organized as follows: Second section briefly describes the study area. In third section the methodology adopted for the data collection and analysis is explained. Fourth section presents the detailed spatial structure of water level, currents and tidal constituents. The relative importance of different nonlinear terms to the momentum balance is examined using a 1D numerical network model. The tidal asymmetry is also analyzed in terms of duration asymmetries in the rise and fall of water level and along-channel transport. In fifth section, the major findings of this study and their implications are discussed. Finally, the paper concludes with key recommendations for future work.

Study area

Cochin estuary is a micro-tidal, geometrically complex estuarine system covering a total area of about 300 km² (Fig. 1). The estuary opens to Arabian Sea through Munambam inlet to the north and Cochin inlet to the middle. Situated parallel to the coast, it can be divided spatially into two arms: (1) the northern arm, extending from Munambam inlet to Cochin inlet (~30 km), and (2) the southern arm, extending from Cochin inlet to Thanneermukkam (~50 km). Munambam inlet has a maximum depth of 4 m and width of about 150 m. The southern arm shallows and widens from a depth of 12 m and width of 450 m at Cochin inlet to 4 m depth and 14 km

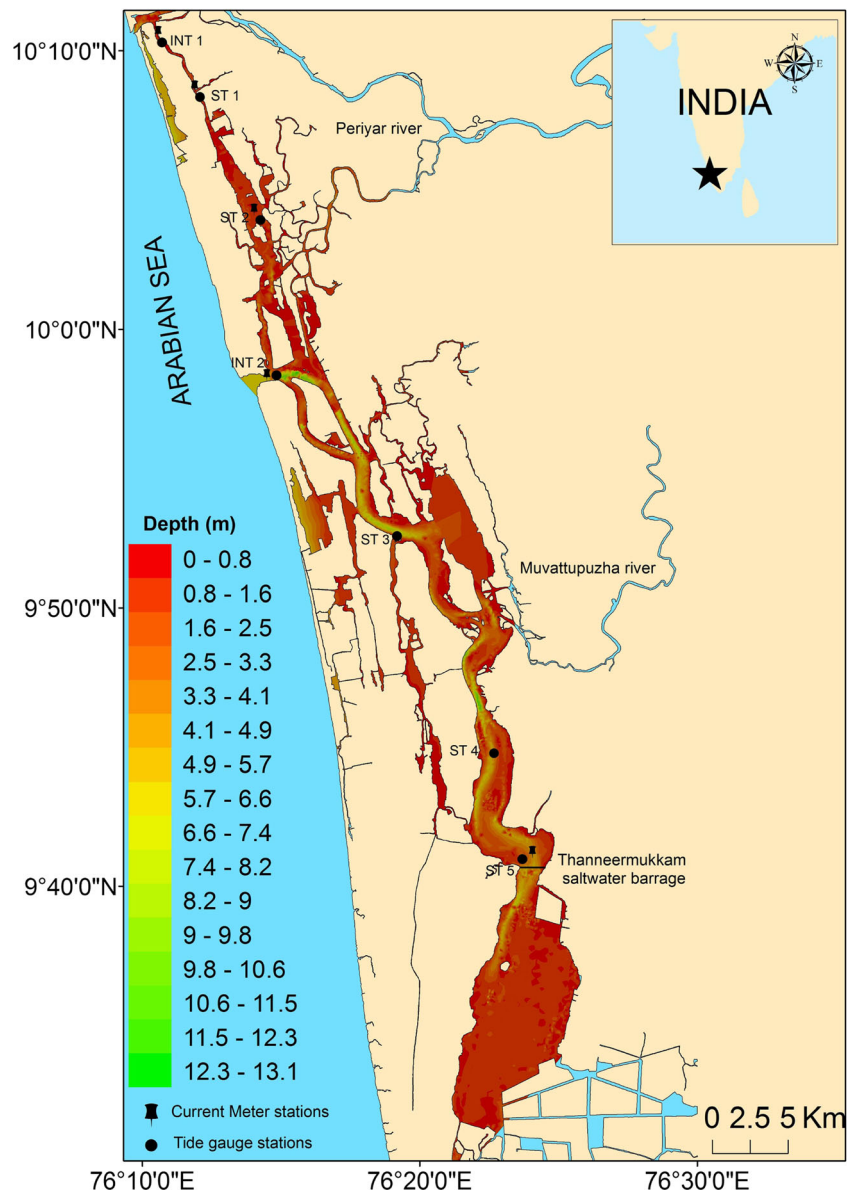
width at Thanneermukkam (depths are reduced to chart datum). The bed roughness coefficient in the estuarine channel is about 55 m^{1/2}/s (Strikwerda 2004) and the bottom sediment texture is characterized by high sand and clay fraction (Nair and Sujatha 2013). The average tidal range of the estuary is 1 m. Six rivers contribute to the freshening of the estuary namely, Periyar, Pamba, Achankovil, Manimala, Meenachil and Muvattupuzha. The Periyar and Muvattupuzha Rivers discharge to the northern and southern arms respectively and the other rivers join upstream, south of the Thanneermukkam Saltwater Barrage. The discharge from Periyar River in to the estuary accounts for only 30 % of its total and the rest flows through Munambam inlet (Shivaprasad et al. 2013a). The highest monthly mean runoff occurs in the wet season (June–September) characterized by Indian Summer Monsoon. The dry season usually prevails from January to May with relatively little runoff. Consequently, the flushing time ranges from 1 to 2.5 days during the wet season and is about 9 days during the dry season (Vinita et al. 2015). According to the Central Water Commission (CWC), the monthly mean discharge varies from 158.75 m³s⁻¹ in February to 1463.83 m³s⁻¹ in July in the year 2010.

Methodology

Data collection and processing

Time series measurements of water level (WL) and currents were carried out for 1 month to document the spatial patterns of tidal flows during the least runoff period. The monthly mean river runoff was 158 m³s⁻¹ in February and 192 m³s⁻¹ in March (CWC 2010). For the field deployment, sampling stations for tide gauges were set up at seven stations: two stations in the proximity of inlets (INT1 and INT2) and five stations (ST1–ST5) along the main channel (Fig. 1). INT1, ST1 and ST2 stations are located in the northern arm whereas INT2, ST3, ST4 and ST5 are in the southern arm of the estuarine channel. Current meters (RCM-9) were deployed midway of the water column depths at INT1, ST1, ST2, INT2 and ST5. Station INT1 was ideally chosen at a distance of 3.6 km inshore from Munambam inlet for instrument deployment. This is because the intermittent rainfall and subsequent discharges from Periyar River catchment area can cause intense flushing through the Munambam inlet which makes measurements practically impossible at the opening. Observations of WL and currents usually began at 0:00 h on 22, February 2010 and ended at 8:00 h on the 22, March 2010. WL data were continuously recorded every 10 min using SBE 26 plus Tide Recorder with

Fig. 1 The map of Cochin estuary. The locations of the tidal gauge and current meter stations are marked



accuracy 0.1 % of full-scale (Strain Gauge Pressure). Simultaneous vertical profiles of current speed and direction were also recorded at 10 min interval using RCM9 current meters. The RCM9 speed sensor has an accuracy of ± 2 % of the recorded speed. Analyses of the data extract the amplitudes and phases of tidal constituents from both WL and current records using software TASK (Tidal Analysis and Software Kit-TASK 2000). Tides and currents were also predicted using TASK for the validation of the observed data. Tide data for offshore stations were extracted using global tidal model.

Numerical modeling

In an effort to understand the relative importance of nonlinear terms to the momentum balance and to examine the spatial

evolution of tidal asymmetry, a 1D numerical model has been used. Nonlinear equations of momentum (Eq. (1)) and continuity (Eq. (2)) in the model are given below:

$$\frac{\partial Q}{\partial t} + \frac{2Q}{A}q - \frac{2bQ}{A} \frac{\partial \eta}{\partial t} = -gA \frac{\partial}{\partial x} (z_0 + d + h) - g \frac{Q|Q|}{AC^2R} \quad (1)$$

$$b \frac{\partial \eta}{\partial t} + \frac{\partial Q}{\partial x} - q = 0 \quad (2)$$

where C is Chezy coefficient calculated using the formula given below:

$$C = \left(\frac{1.49}{n} \right) R^{1/6} \quad (3)$$

and t , x , Q , η , q , g , d , and n are respectively, time, along-channel coordinate (increasing in upstream direction), along-

channel transport, elevation with respect to mean WL, freshwater influx per unit channel length, acceleration due to gravity, depth and manning coefficient; z_0 is the height between bottom of the channel and an arbitrary datum below the bottom; b is the width of the channel through which the horizontal flow occurs including mud flats which act as storage; R is the hydraulic radius (A/P_r) where P_r is the wetted perimeter and A is the area of cross section. The first and second terms on the right-hand side of Eq. (1) represent, respectively, pressure gradient and friction. On the left-hand side, the first term represents temporal acceleration and the rest of the terms are non-linear advection. In the momentum Eq. (1), the non-linear term $u^2 \frac{\partial A}{\partial x}$ is omitted from the equation due to its negligible importance in most estuaries and canals. For a rectangular channel of variable area, $A=b(d+\eta)$

$$u^2 \frac{\partial A}{\partial x} = g \left(\frac{u}{c}\right)^2 A \frac{\partial(d+\eta)}{\partial x} \quad (4)$$

where c is the speed of the gravity wave given by $c = (g \frac{A}{b})^{\frac{1}{2}}$. In Cochin estuary, the maximum value of $(\frac{u}{c})^2$ found is about $0.003 \ll 1$ and hence the final form of the non-linear momentum equation does not contain this term. Derivation of the equations has been given by Harleman and Lee 1969. Equations (1) and (2) are solved using the finite difference scheme on an Arakawa C-grid. The model grid resolution is 1000 m and the time interval is 30 s. The model was initialized with zero surface elevations and velocities. To force the model, observed time series measurements of WL were prescribed at the open boundaries (INT1 and INT2) as a function of time. The monthly mean runoff was prescribed at interconnecting grids of rivers and the main channel.

In order to evaluate the model quantitatively against the measured WL, two performance metrics: correlation coefficient (R) and skill score (SS) were utilized. The expression of correlation coefficient R, which measures the linear relationship between the model and the observations, is given below:

$$R = \sigma_m^{-1} \sigma_0^{-1} \frac{1}{N} \sum_{i=1}^N (X_{m,i} - \bar{X}_m) (X_{0,i} - \bar{X}_0) \quad (5)$$

where X_m and X_0 are the values from the model and observations respectively, an overbar represents a time average, N is the number of observations, and σ_m and σ_0 are the standard deviations of the model and observations (Ralston et al. 2013). The model skill score (SS) depends on the root-mean-square error between the model and observations normalized by the standard deviation of the observations (Murphy 1988):

$$SS = 1 - \sigma_0^{-2} \frac{1}{N} \sum_{i=1}^N (X_m - X_0)^2 \quad (6)$$

The maximum SS is 1 when the model exactly agrees with the observations. An SS of 0 indicates that the model provides equal predictive skill as assuming the mean of the observations, and a negative SS indicates that the model is less predictive than the mean of the observations.

Tidal asymmetry

Since tidal current measurements were limited to few locations in the estuary, the tidal asymmetry was quantified in terms of tidal duration using WL data. Moreover, this approach is advantageous because bathymetry can produce local asymmetries in tidal currents that are generally not seen in the free surface record (Godin 1991). Following Nidzieko (2010), tidal duration asymmetry was quantified for the full length of WL records via the normalized sample skewness of the WL time derivative ($\frac{\partial \zeta}{\partial t} = \zeta'$):

$$\gamma_1 = \frac{\mu_3}{\sigma^3} = \frac{\frac{1}{\tau-1} \sum_{t=1}^{\tau} (\zeta'_t - \bar{\zeta}')^3}{\left[\frac{1}{\tau-1} \sum_{t=1}^{\tau} (\zeta'_t - \bar{\zeta}')^2 \right]^{3/2}} \quad (7)$$

where μ_3 is the third sample moment about the mean and σ is the standard deviation, the square-root of the second sample moment about the mean. The summation is for t observations from time $t=1$ to $t=\tau$. Ebb-tide duration is shorter for $\gamma_1 < 0$ and flood-tide duration is shorter for $\gamma_1 > 0$. This method was adopted for the tidal asymmetry analysis as it is not sensitive to record length unlike harmonic methods. In order to quantify tidal asymmetry relevant to sediment transport, skewness was also computed for the along-channel transport $Q(t)$ in momentum Eq. (1) simulated using the numerical model for the five stations.

Results

Water level and currents

The observed and predicted WL are shown in Fig. 2. It demonstrates the spatial and spring-neap variability of WL with diurnal inequality. The average diurnal inequality was about 11.4 cm and the largest (15 cm) occurred at the inlet stations (INT1 and INT2). The WL amplitude peaked to 50 cm at these stations; INT1 showing marginally higher values (53 cm) owing to channel convergence. Inside the estuary at about 4.5 km from the Munambam inlet, the WL dropped to 27 cm at ST1. At ST2, the tides propagated from Cochin inlet and the WL increased to 36 cm. At the southern arm, the WL was 31 cm at ST3 and slightly got amplified to 35 cm at ST4 due to channel

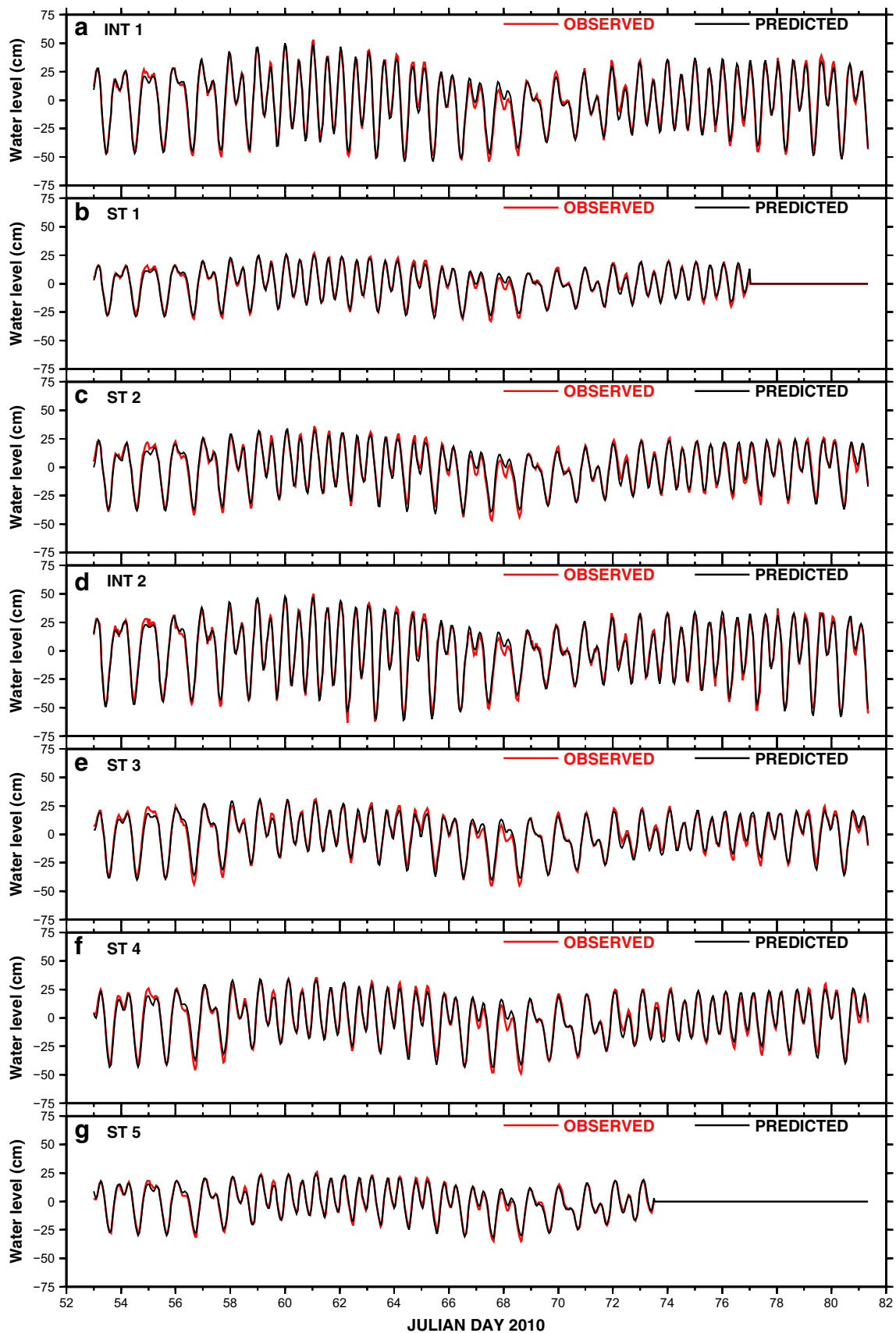


Fig. 2 Time series of observed and predicted water level at seven stations in the estuary

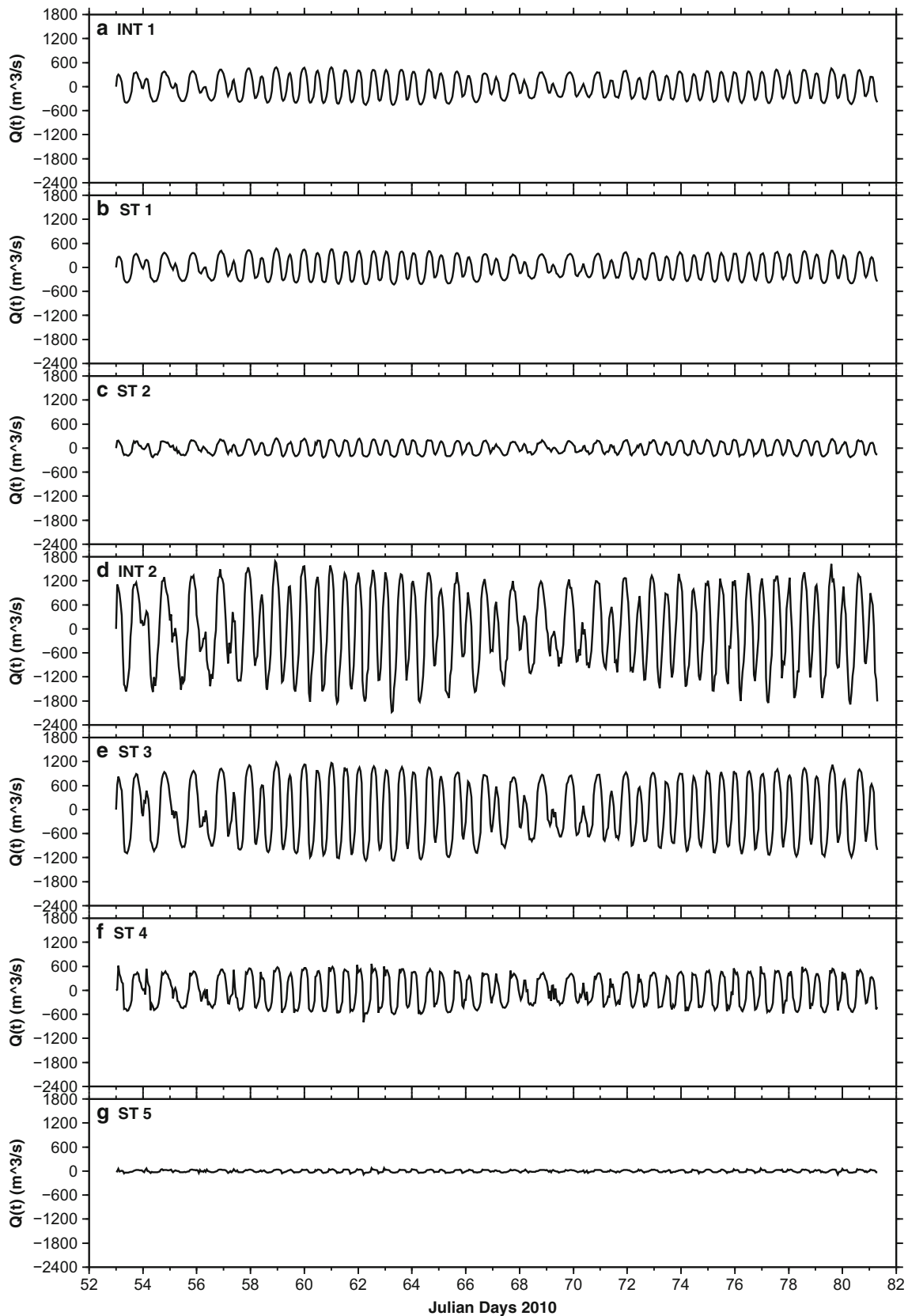


Fig. 3 Time series of along-channel transport $Q(t)$ simulated using 1D numerical model for seven stations in the estuary

convergence. Towards the widespread upstream regions, WL was greatly attenuated to 26 cm at ST5 station.

The diurnal inequality and spring-neap variability observed in tides were also imprinted on current records. The measurements showed that the maximum observed mean velocities occurred at INT1 (29 cm s⁻¹) and INT2 (27 cm s⁻¹), respectively. In the northern arm, the mean velocities were 14.1 cm s⁻¹ at ST1 which decreased to 8.4 cm s⁻¹ at ST2. The lowest mean currents were recorded at ST5 far upstream. At INT1, the water flow was dominated by the southeast-northwest direction (130°–300° with respect to true north). At ST1, the direction of flood was 240° and that of ebb was towards INT1. At ST2, the direction of flow reversed at this station. The flood flow was directed towards northern inlet (330°) and the ebb flow towards Cochin inlet (140°). Due to the orientation of the channel along the east–west direction at INT2, the flood-ebb flow was dominated in the northeast-southwest direction (91°–250°). At ST5, the flood currents were directed south whereas the ebb flowed towards INT2. It was seen that among the observed currents, *v*-components were dominant at all stations except ST2 and ST5. While the observed mean *u*-components (24.5 cm s⁻¹) were greater than *v*-components (14.2 cm s⁻¹) at ST2, they were akin at ST5 (11 cm s⁻¹). The along-channel transport *Q*(*t*) obtained from Eq. (1) using the numerical model simulations are shown in Fig. 3. There was decrease in the transport towards upstream owing to the decrease in the strength of the tidal currents. The maximum value of mean *Q*(*t*) was found at INT2 (850 m³ s⁻¹) followed by ST3 (673 m³ s⁻¹). The least value of *Q*(*t*) occurred at ST5 showing 24 m³ s⁻¹.

Table 1 lists the pertinent details of the properties of observed WL and currents for a spring tidal cycle in March 2010 (Fig. 4a). Evidently, the time delay of high water between different stations in the estuary is shorter than the time delay of low water. Notably, the delay in high water from INT2 to ST5 was 2 h and 50 min whereas during low water it was 3 h and 20 min. Almost symmetrical tides with respect to duration and velocity were attained in INT1. On the contrary, at INT2, stronger ebb

currents for longer duration were observed. At all the other stations flood currents were stronger with shorter duration.

Tidal harmonics

Tidal amplitudes and Greenwich phases for the constituents of WL are given in Table 2. The amplitude and phases of the tidal harmonics along the main channel reveal a steady change in the character of the tides from the inlet towards the upstream of the estuary. About 96–98 % of observed WL variance could be explained by tidal harmonics suggesting that the non-tidal influences were the least during the observation. Particularly significant were the M2 and K1 harmonics along the estuary. The third most important was S2 followed by O1. At the inlets, amplitudes of M2 and K1 were nearly equal with 23 and 22 cm respectively, whereas K1 was slightly dominant at the other stations. Maximum dominance of K1 over M2 (1.5 cm) was observed at ST3 station. The tidal form number was calculated using the expression $N_f = (K1+O1)/(M2+S2)$ (Defant 1960). N_f was 0.97 at INT1; 1.14 in the northern arm stations; ST1 and ST2. In southern arm, this ratio was 0.99 at INT2; 1.42 at ST3; 1.22 at ST4; 1.18 at ST5 indicating mixed, predominantly semidiurnal tides. Phase lags of tidal constituents gradually increased from inlet toward upstream and remained close to the same value at the upstream end of both the arms. Phase lag of M2 along the main channel is about 3.54 h from the mouth to 44 km inland and it was slightly more at INT1 than at INT2. The largest higher harmonics generated in the estuary are MK3, MS4 and M4. In the northern arm, the maximum observed amplitude of MK3 was 2.1 cm at ST2. The amplitude of MK3 at INT2 was 1 cm which dropped at ST3 and remained relatively constant at the upper estuary. However, both MS4 and M4 harmonics were the highest at INT2 with amplitudes of 1.5 cm and 1.8 cm respectively.

The tidal ellipse parameters of dominant constituents and the tidal transport formed as a product of cross-sectional area and major axis amplitude are shown in Table 3. The narrow main channel of the estuary confines the motion of the tidal currents into nearly rectilinear forms. Hence we focused on

Table 1 Properties of observed water level and currents for a spring tidal cycle in March 2010

Stations	Tidal range/ depth (a/h)	T _{HS}	T _{LS}	T _{HWS}	T _{LWS}	Peak flood velocity(cm/s)	Peak Ebb velocity(cm/s)	Duration of Ebb (min)	Duration of flood (min)
INT1	0.3	1:00	07:00	02:20	09:00	58.6	62.5	410	400
ST1	0.3	1:30	08:20	02:50	09:30	34.3	13.4	400	350
ST2	0.4	02:00	09:30	03:00	09:50	25.8	16.7	410	370
INT2	0.07	01:00	06:20	01:20	09:40	36.6	47.2	520	260
ST3	0.2	02:40	09:40	–	–	–	–	–	–
ST4	0.3	03:30	10:40	–	–	–	–	–	–
ST5	0.3	03:50	09:40	03:80	10:30	7	4.6	420	370

THS Time of High Stand, *TLS* Time of low stand, *THWS* Time of high water slack, *TLWS* Time of low water slack

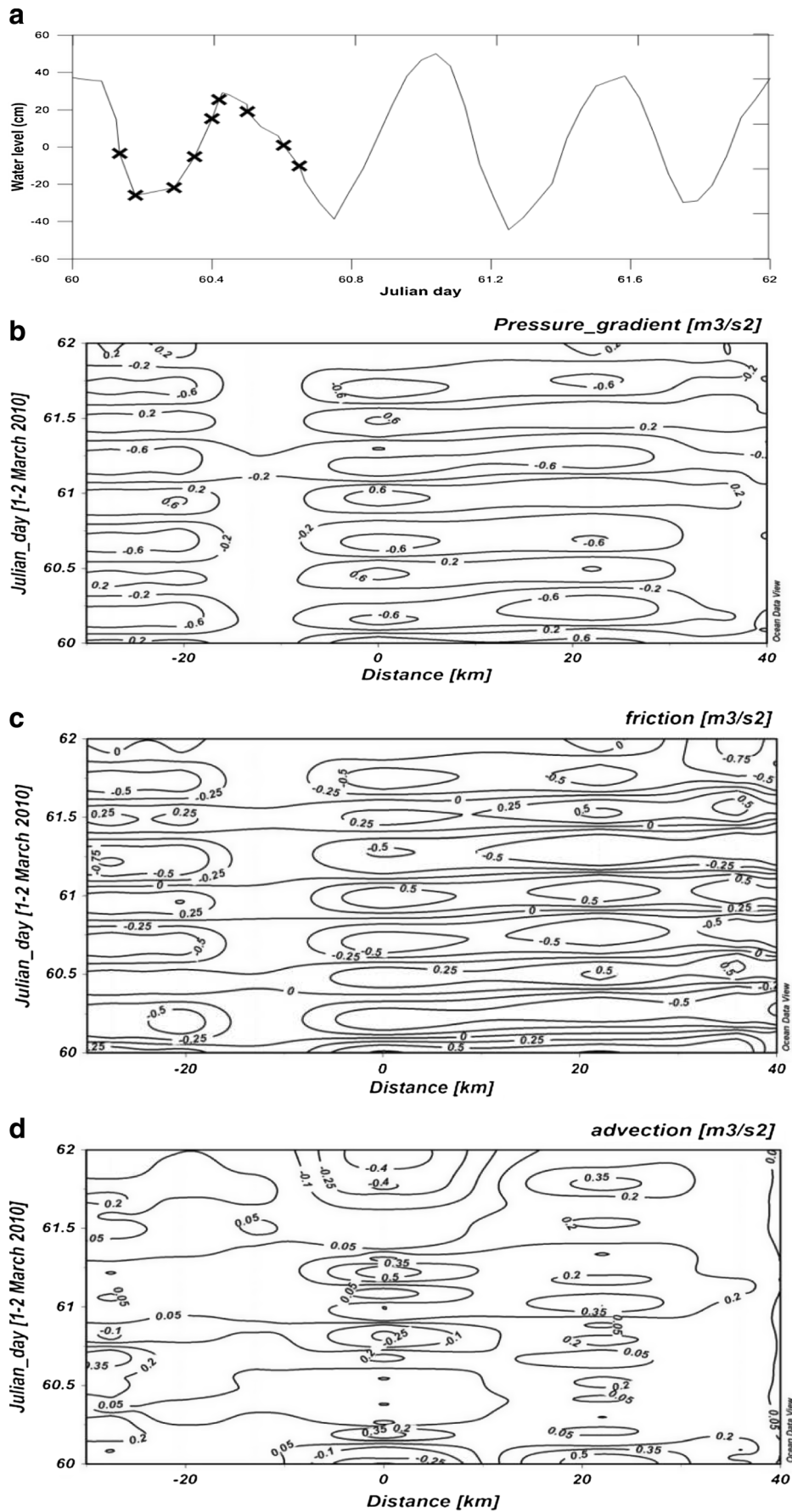


Fig. 4 **a** Observed water level at Cochin inlet station (INT2) for 1–2 Mar 2010 (spring phase). **(b–d)** Contour plots of **(b)** pressure gradient, **(c)** friction and **(d)** non-linear advection terms in the momentum balance (Eq. 4) during the same period of spring tide shown in **(a)**. The *horizontal axis* shows distance (km) along the main channel and the *vertical axis* shows Julian days. The contours are in units of $\text{m}^3 \text{s}^{-2}$

the major axis of the tidal ellipses for the analyses. The dominant semi-diurnal and diurnal ellipses were M2 and K1, respectively. At INT1, the ellipses were strongly elongated and inclined to the coastal line. The M2 major-axes amplitudes were greatest reaching 37.2 cm s^{-1} followed by K1 with 22.05 cm s^{-1} . At ST1, the ellipses were inclined at an angle of 200° (rotated counter clockwise from east) whereas they became quasi-parallel to coastal line at ST2. At INT2, M2 and K1 ellipses were substantial reaching 17.47 and 11.41 cm s^{-1} respectively and oriented at 40° . There was a sharp reduction in the amplitude of major axis of all ellipses at ST5 where M2 ellipses were dominant with amplitude of 1.59 cm s^{-1} . Average ratio of S2 to M2 semi-major axes was 0.35, indicating a pronounced spring-neap cycle. Form number of tidal currents was calculated using major axes amplitudes, which was measured as 0.58 at INT1; 0.60 at ST1; 0.86 at ST2 in northern arm. At southern arm, it was 0.61 at INT2 and 0.57 at ST5. All the current form numbers were smaller than their respective tidal form number, indicating that the currents were mixed and predominantly semidiurnal. The eccentricities of current ellipses were generally found to be nearly zero resulting in rectilinear currents. They became more elliptical towards upstream stations ST2 (0.13) and ST5 (0.54) stations where channel widths are larger compared to downstream regions. Hence, the sense of rotation of the ellipses was particularly important at these stations. At ST2, ellipses of diurnal and semidiurnal constituents rotated in clockwise direction whereas at ST5 diurnal ellipses rotated in clockwise and semidiurnal ellipses rotated in counterclockwise directions. The tidal transport reveals a regular decrease in the upstream

direction. The maximum tidal transport was obtained for M2 followed by K1. It varied from $1038 \text{ m}^3 \text{ s}^{-1}$ for M2 at station INT2 to $6 \text{ m}^3 \text{ s}^{-1}$ for S2 and K1 at station ST1.

Numerical model and momentum budget terms

Table 4 shows the comparison of the modeled and observed amplitudes and phases of M2. The difference in amplitude between the model and the observations was less than 15%. The numerical model performance was further assessed quantitatively using the metrics defined in Eqs. (5 and 6). The WL at all stations was well captured by the model, with high correlations (0.83–0.99). Close to the inlets, both the R^2 and SS values were found to be extremely high (>0.99). At all the other stations R^2 and SS values ranged from 0.93–0.99 except at station ST2. Here, the WL was reproduced with R^2 value of 0.83 and a moderate SS of 0.69.

To examine momentum balance in the model, the contribution of each of the three terms (nonlinear advection, pressure gradient and friction) to momentum balance during a spring tidal cycle (Fig. 4a) was evaluated. Contribution of each term during the tidal cycle is shown in Fig. 4b–d. These figures show that near the upstream regions, the momentum balance is entirely between pressure gradient and friction (Fig. 4b–c). Towards the mouth, contribution of non linear advection increases (Fig. 4d), but its magnitude was smaller than the other two terms. WL simulations using the numerical model for the time marked in Fig. 4a are shown in Fig. 5. With the tides propagating upstream, the WL changed in accordance with the shape of the estuarine channel. It can be noted that the WL amplitudes were greater in southern arm compared to northern arm. The decrease in amplitudes towards upstream was about 83% compared to INT2. The time series of WL computed by the model also showed phase lags similar to that of the observed tides. It can be noted that the differences between WL at INT2 and upstream stations was

Table 2 Amplitudes (A) and phase angles (Φ) of the significant tidal constituents for Cochin estuary by harmonic analysis of water level data in 2010 peak dry season

Tide	Stations													
	INT1		ST1		ST2		INT2		ST3		ST4		ST5	
	A	Φ	A	Φ	A	Φ	A	Φ	A	Φ	A	Φ	A	Φ
O1	9.3	58.2	5.8	66.9	7.1	71.6	10.2	60.1	7.7	78.9	7.7	86.6	6.7	81.9
K1	21.6	65.9	12.8	82.5	17.2	92	22.1	58.8	18.7	98.5	18.7	105.3	11.3	104.2
M2	23.6	343.9	12.6	9.5	16.2	23.5	23.5	336.2	13.5	43	17.2	66.3	12.1	71
S2	7.9	36.6	3.7	62.6	4.6	80.2	9.0	30.1	3.0	101	4.4	134.2	3.1	139.1
MK3	0.6	303.2	1.0	322.7	2.1	339.8	1.0	138.3	0.2	27.2	0.9	87.2	0.8	93.5
MS4	0.1	31.2	0.3	216.9	1.0	278.2	1.5	135.2	0.2	11.1	0.8	126.2	0.8	356.1
M4	0.5	111.5	0.3	216.9	1.0	278.2	1.8	82.7	0.4	225.7	0.7	0.68	0.8	356.1

A amplitude (cm), Φ phase (degrees)

Table 3 Tidal ellipse parameters and tidal transport for major tidal constituents at 5 stations

Stations	sema (m s ⁻¹)	ecc	inc (deg)	Tidal transport (m ³ s ⁻¹)	sema (m s ⁻¹)	ecc	inc (deg)	Tidal transport (m ³ s ⁻¹)
	M2				K1			
INT1	0.372	-0.003	320	222	0.22	0.021	320	131
ST1	0.190	0.007	200	19	0.09	-0.004	202	9
ST2	0.088	-0.049	109	230	0.073	-0.130	119	192
INT2	0.175	-0.009	40	1038	0.114	-0.038	43	678
ST5	0.016	0.195	316	95	0.003	-0.541	337	19
	S2				O1			
INT1	0.132	0.033	320	79	0.074	0.108	320	44
ST1	0.064	0.021	201	6	0.063	-0.001	201	6
ST2	0.030	-0.084	115	80	0.029	-0.004	113	76
INT2	0.066	0.002	42	391	0.034	-0.043	36	204
ST5	0.006	0.246	308	36	0.009	-0.173	4	57

Notations sema, ecc, inc stands for semi major axis, eccentricity and angle of inclination. (-) for ecc indicates clockwise rotation for tidal ellipse

about 10 cm at low tides (Fig. 5b) and 1.8 cm at high tides (Fig. 5f). Hence, the surface gradient was steeper towards upstream at low tides than at high tides.

Tidal duration asymmetry

The tidal duration asymmetry was quantified via skewness (Eq. (7)) of the observed and simulated tides for all the seven stations. Additionally, tides were constructed using the principal constituents M2, K1 and O1 alone and re-constructed after including higher harmonics (MK3, M4). Skewness was evaluated for both these tides and the results are shown in Fig. 6. The skewness of the simulated tides was in good agreement with the observed tides suggesting that the model could capture the geometrical features within the estuary reasonably well. There is a decrease in the asymmetry caused by principal tides with distance from inlets. However, the effect of non-linearities on asymmetry was found to be increasing

toward upstream. With just the principal tides M2, K1, and O1, the tidal duration asymmetry was flood-dominant. When M4 and MK3 harmonics were included, the asymmetry changed markedly. At INT1, the asymmetry of the principal tides alone (0.07) and of the tides constructed with higher harmonics (0.10) matched with the asymmetry of observed tides (0.11). At all the other stations of northern arm, there was extreme influence of higher harmonics which reinforced the asymmetry of the principal tides leading to flood dominance in the observed tide. In contrast, the observed tidal asymmetry at INT2 transformed to ebb dominance ($\gamma_1 = -0.35$). Here, although the principal tides were flood dominant ($\gamma_1 = 0.18$), with the addition of higher harmonics the tides turned to be ebb dominant ($\gamma_1 = -0.23$). Station ST5 was largely flood dominant with $\gamma_1 = 0.45$. Skewness computed for Q(t) simulated using the model (Fig. 3) is also shown in Fig. 6. It was found that while stations INT2 and ST3 showed ebb dominant transport, all the other stations were flood dominant.

Skewness was also evaluated for tides predicted for the same period of observation at a distance of about 12 km offshore of the inlet stations (INT1 and INT2). These tides were found to be weakly flood dominant ($\gamma_1 = 0.06$). Figure 7 depicts the skewness computed from WL simulated for 1 month, throughout the estuary. Flood dominance prevailed in all regions along the northern arm with γ_1 values ranging from 0.11 to 0.19. Along southern arm, by contrast, the lower reaches were ebb dominant with γ_1 values ranging from -0.36 to -0.01. There was an increase in ebb dominance towards in-shore and further inland at about 8 km distance, the tides switched to flood dominance. Flood dominance increased towards the shallow and wide regions upstream with maximum γ_1 values of 0.39.

Table 4 Comparison of observed and modeled M₂ amplitudes (A_{obs} , A_{mod}) and phases (Φ_{obs} , Φ_{mod})

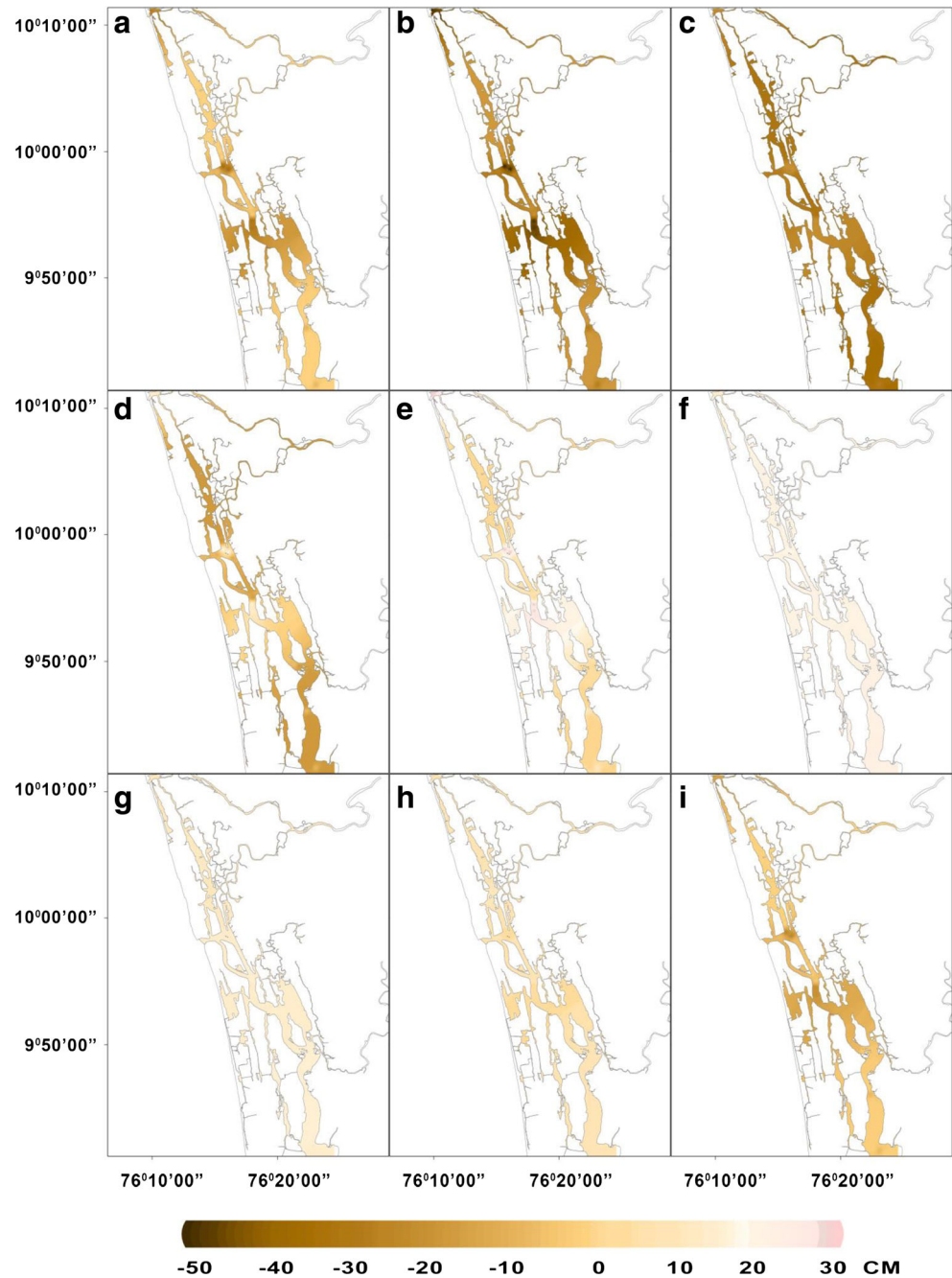
Stations	A_{obs} (cm)	A_{mod} (cm)	$ \delta A $ (cm)	Φ_{obs} (cm)	Φ_{mod} (cm)	$ \delta \Phi $ (cm)
INT1	23.6	22.9	0.7	343.9	346.2	2.3
ST1	12.6	10.9	1.7	9.5	10.7	1.2
ST2	16.7	15.3	1.4	23.6	30.8	7.2
INT2	23.5	23.2	0.3	336.2	338	1.8
ST3	13.5	11.9	1.6	43	69.8	26.8
ST4	17.2	15.5	1.7	66.3	30.7	35.6
ST5	12.1	12.1	0	71	70.8	0.2

Discussion and conclusion

Estuaries on the west coast of India are generally convergent towards upstream regions. In such estuaries (eg., Mandovi estuary), the geometric amplification arising from convergence of the estuarine channel from mouth to head balances frictional dissipation to sustain the undamped propagation (Unnikrishnan et al. 1997). On the other hand, the width of the Cochin estuary increases towards upstream, consequently, the amplitude of tides and currents get decayed through both friction and non-linear transfers of energy, thus the estuary is

hyposynchronous. M2 and K1 were the most representative components and a competing dominance of M2 over K1 was observed throughout the estuary. The third most important was S2 followed by O1. Along-channel width variations and bathymetric gradients were the major source of ellipticity changes of tidal currents. The distortion of astronomical tides gave rise to the most significant higher harmonics MK3, MS4 and M4. There was no consistent increase in the higher harmonics towards upstream indicating that the local bathymetry and topography induced large spatial variability in the generation of higher harmonics.

Fig. 5 Spatial water level fluctuations simulated using numerical model during spring tide (1–2 Mar 2010) at times marked as X's in Fig. 4a



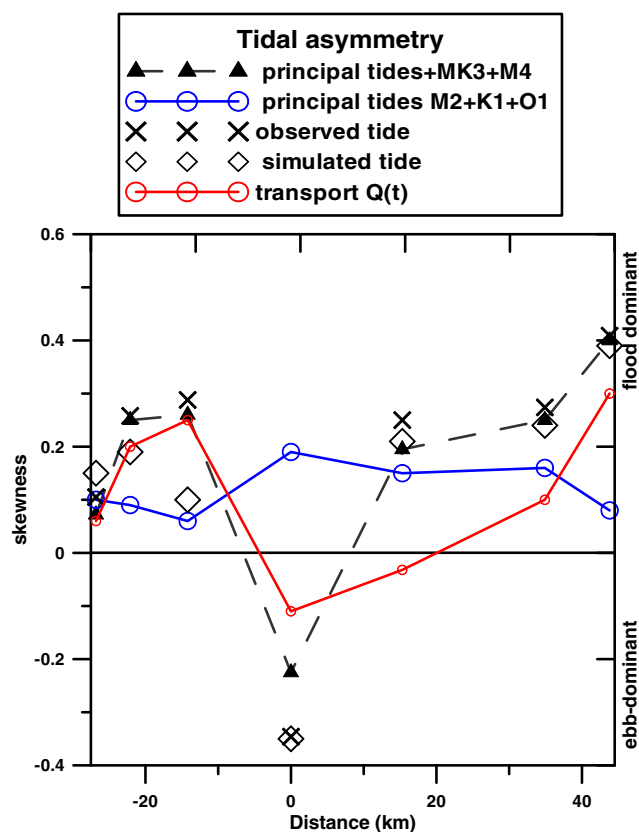


Fig. 6 Asymmetry as function of distance along-channel for Cochin estuary. Skewness (γ) computed from principal tides + MK3+ M4 (\blacktriangle \blacktriangle), principal tides M2+ K1+O1 (\bigcirc \bigcirc), observations (\times \times), simulated tides (\diamond \diamond) and along-channel transport $Q(t)$ (\bigcirc \bigcirc)

The relative importance of different non-linear terms for the momentum balance was investigated using a numerical model. The model achieved high skill against time series of WL and the response of tidal character to the channel geometry was clearly captured. Tidal momentum balance along the main axis of the channel was dominated by pressure gradient and friction. Near both inlets, non-linear advection was also found significant which was negligibly low in other parts of the estuary. The driving nonlinearities for overtides and compound tides in the equation of momentum are non-linear advection and bottom friction (Giese and Jay 1989; Parker 1991). It was observed that friction was dominant over advection contributing towards most of the tidal distortions at all stations. The rapid decay in the tidal amplitude can also be caused by the freshwater discharge originating at the upstream. However, during the dry season, in Cochin estuary, the river discharge originating upstream is zero due to the closure of Thanneermukkam Saltwater Barrage.

The tidal asymmetry was quantified in terms of statistical skewness. Offshore tides entering the estuary through both inlets prior to any distortion were found to be weakly flood-dominant. At INT1, the amplitudes of higher harmonics were

not large enough to produce any effect on the asymmetry of principal tides. Thus, the total observed asymmetry at INT1 was primarily contributed by the offshore tidal forcing. However, with increase in distance, the non-linearity increased and consequently the asymmetry imposed by higher harmonics to skewness became dominant. The tidal dynamics of southern arm differs from that of the northern arm. The along-channel transport $Q(t)$ was relatively higher in the southern arm (Fig. 3). All the non-linear mechanisms intensified at the main inlet (INT2) increasing the potential for generation of higher harmonics. As a result, the weak flood dominant forcing of the offshore tides was transformed to ebb dominance. It was also found that although the principal tides were flood dominant, with the addition of higher harmonics the asymmetry shifted to ebb-dominance. This indicates that the observed ebb-dominant asymmetry was a result of local topographic influences. There is an increase in ebb-dominance towards inshore associated with the increase in non-linearity and the tides do not become flood dominant until beyond 8 km (Fig. 7). From this location to upstream reaches, the depths decrease abruptly from ~ 6 to ~ 2 m and the shallow areas cause enhanced flood dominance due to friction.

The tidal asymmetries dictated by the skewness were clearly observed in the characteristics of the observed water level and currents of all stations except INT2 (Table 1). The observed tides at INT1 were almost duration symmetrical as substantiated by the smallest skew of 0.11 (weak flood dominance) obtained for this station. On the contrary, strong ebb currents and longer ebb duration were observed at INT2. Despite the fact that the river discharge originating upstream is negligible during dry season (Shivaprasad et al. 2013b), Muvattupuzha River and several other tributaries (Fig. 1) joining along the channel contributes towards the freshening of the estuary. The freshwater input from these tributaries is sufficient to impose an ebbward pressure gradient that prolongs the duration of the ebb phase. This makes the ebb phase stronger and longer as opposed to the classical definition of shorter but stronger ebb flow in ebb dominant system.

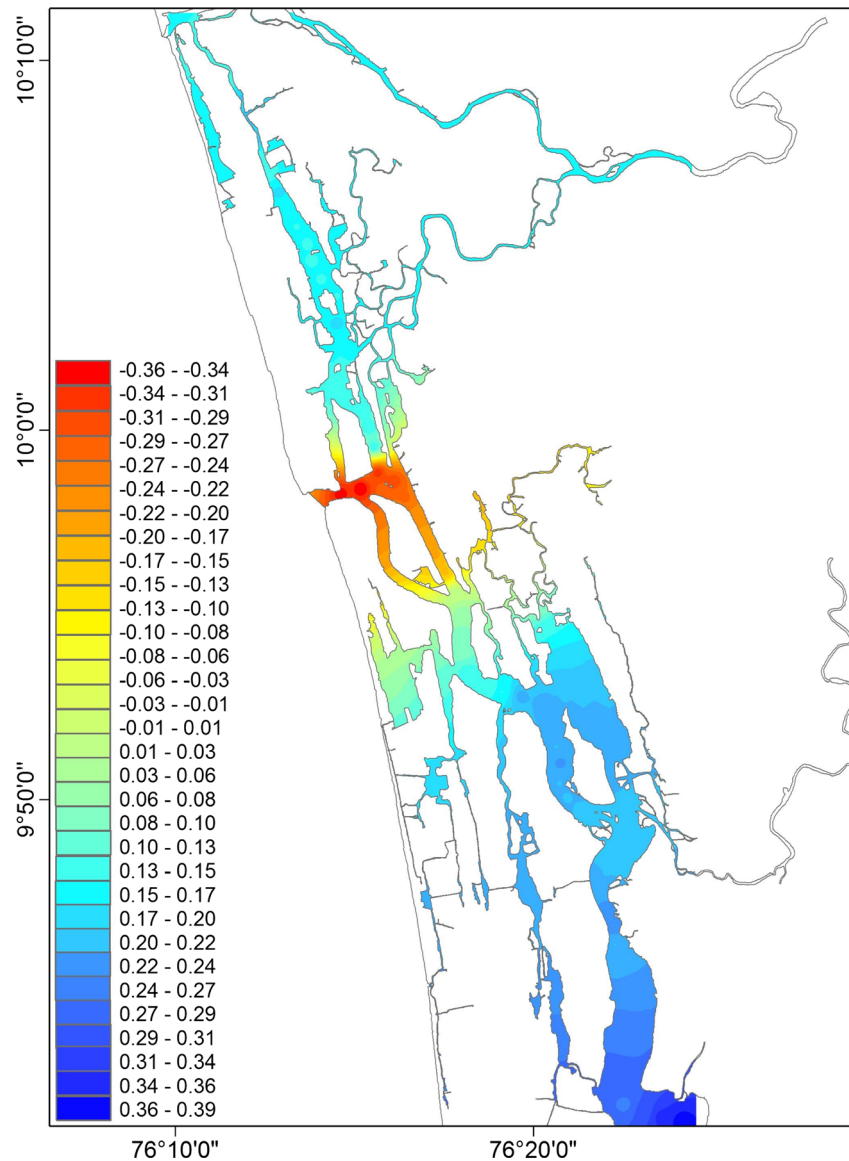
A number of researchers have pointed out that (Dronkers 1986; Friedrichs and Aubrey 1988; Prandle 2003; Robins and Davies 2010), non-linear friction cause greater frictional damping in shallow water, slowing the propagation of water level changes around low tide relative to high tide. Thus the time delay between low water at the inlet and low water in the inner estuary is greater than the time delay between high waters. This results in a longer, weaker ebb tide and a shorter, stronger flood tide (due to conservation of mass) and hence, potentially, flood dominance. Therefore, an estuary is likely to become more flood-dominated as the tide propagates landward where the a/h ratio increases. This is consistent with our observations as the time delay between the low tide at the inlets and low tide in the upper estuary was found to

be greater than the time delay between high tides (Table 1). With the increase in a/h ratio, flood dominance increased towards upstream (Figs. 6 and 7). However, considering the sea level set-up in the estuary, ebb dominant velocities can be found at the immediate vicinity of the inlets (Friedrichs et al. 1992). This is because due to the larger differences between inlet and upper estuary in low water compared to high water, a much steeper surface gradient occurs near low water (Fig. 5). Therefore, ebb dominance in $Q(t)$ was found at the main inlet INT2 and ST3, the station adjacent to it. Moreover, the effect can be accelerated by the deepening of channels. Intense dredging maintains an average depth of 10 m in the harbor area ($\sim 9.5 \text{ km}^2$) at the lower reaches of the estuary which can modify the tidal asymmetry in that area (Fig. 7). The morphological changes induced by dredging operations can alter the nature of the tidal asymmetry from flood

dominance to ebb-dominance thereby promoting sediment flushing to sea (Oliveira et al. 2006; Colby et al. 2010). Thus, Cochin estuary has an ebb dominant mouth region to flood dominant main channels.

The results of this study have implications for management within estuaries and sediment transport mechanisms, particularly where dredging may change the morphology and could potentially shift an accreting, flood dominant system to an eroding ebb dominant system. Sediment transport is roughly proportional to velocity cubed (Gadd et al. 1978), so skewness calculation for a velocity time series provides a more relevant metric for sediment transport potential. Moreover, during Indian monsoon season the rivers deposit large amount of sediment loads in to the estuarine channel leading to siltation in the harbor area (Balchand and Rasheed 2000). Therefore, for future research it is recommended to

Fig. 7 Skewness (Υ) computed for the simulated tides in the entire estuary during dry season



investigate the seasonal variations in tidal velocity skew and its relationship with the estuarine morphology which can be achieved utilizing simultaneous time series velocity records of multiple stations.

Acknowledgments The authors would like to thank the director of the National Institute of Oceanography (NIO), Goa, and the scientist in-charge of the NIO Regional Centre, Cochin, for support and encouragement. This paper work is a part of the doctoral research of the first author, Vinita J. who acknowledges the Council of Scientific and Industrial Research, New Delhi, for the financial support in the form of a senior research fellowship. This research was also partially funded by the Integrated Coastal and Marine Area Management under the project “Ecosystem Modeling of Cochin Estuary”. This is NIO’s contribution 5779.

Compliance with Ethical Standards

Conflict of interest The authors declare that they have no conflict of interest.

Human and Animal Rights and Informed Consent This article does not contain any studies with human participants or animals performed by any of the authors.

Informed consent was obtained from all individual participants included in the study.

References

- Balachandran KK, Reddy GS, Revichandran C, Srinivas K, Vijayan PR, Thottam TJ (2008) Modelling of tidal hydrodynamics for a tropical ecosystem with implications for pollutant dispersion (Cochin Estuary, Southwest India). *Ocean Dyn* 58:259–273
- Balchand AN, Rasheed K (2000) Assessment of short term environmental impacts on dredging in a tropical estuary. *Terra Aqua* 79
- Blanton JO, Lin G, Elston SA (2002) Tidal current asymmetry in shallow estuaries and tidal creeks. *Cont Shelf Res* 22:1731–1743
- Colby LH, Maycock SD, Nelligan FA, Pocock HJ, Walker DJ (2010) An investigation into the effect of dredging on tidal asymmetry at the river murray mouth. *J Coast Res* 26(5):843
- Defant A (1960) *Physical oceanography*, 2. Peragamon Press, Oxford, 598 pp
- Dronkers J (1986) Tidal asymmetry and estuarine morphology. *Neth J Sea Res* 20:117–131
- Friedrichs CT, Aubrey DG (1988) Non-linear tidal distortion in shallow well-mixed estuaries: a synthesis. *Estuar Coast Shelf Sci* 27:521–545
- Friedrichs CT, Lynch DR, Aubrey DG (1992) Velocity asymmetries in frictionally-dominated tidal embayments: longitudinal and lateral variability. In: Prandle D (ed) *Dynamics and exchanges in Estuaries and the Coastal Zone*. Springer, New York, pp 277–312
- Gadd PE, Lavelle JW, Swift DJP (1978) Estimates of sand transport on the New York shelf using near-bottom current meter observations. *J Sediment Petrol* 48:239–252
- Gallo MN, Vinzon SB (2005) Generation of overtides and compound tides in Amazon estuary. *Ocean Dyn* 55:441–448. doi:10.1007/s10236-005-0003-8
- Giese BS, Jay DA (1989) Modelling tidal energetics of the Columbia River Estuary. *Estuar Coast Shelf Sci* 29(6):549–571
- Godin G (1991) The analysis of tides and currents (review). In: Parker BB (ed) *Tidal hydrodynamics*. Wiley, New York, pp 675–708
- Harleman DRF, Lee CH (1969) The computation of tides and currents in estuaries and canals. Technical bulletin 16, M.I.T., Massachusetts, 264 pp
- Hoitink AJF, Hoekstra P, Van Maren DS (2003) Flow asymmetry associated with astronomical tides: implications for the residual transport of sediment. *J Geophys Res* 108(C10):3315. doi:10.1029/2002JC001539
- Kumar PKD, Gopinath G, Murali RM, Muraleedharan KR (2013) Geospatial analysis of long-term morphological changes in Cochin estuary, SW coast of India. *J Coast Res*. doi:10.2112/JCOASTRES-D-12-00244.1
- Manoj NT, Unnikrishnan AS, Sundar D (2009) Tidal asymmetry in the Mandovi and Zuari Estuaries, the West Coast of India. *J Coast Res* 25(6):1187–1197
- Murphy AH (1988) Skill scores based on the mean square error and their relationships to the correlation coefficient. *Mon Weather Rev* 116:2417–2424
- Nair MP, Sujatha CH (2013) Environmental geochemistry of core sediment in the Cochin Estuary (CE). *India Res J Chem Sci* 3(4):65–69
- Nidzicko NJ (2010) Tidal asymmetry in estuaries with mixed semidiurnal/diurnal tides. *J Geophys Res* 115. doi:10.1029/2009JC005864
- Oliveira A, Fortunato AB, Regob JRL (2006) Effect of morphological changes on the hydrodynamics and flushing properties of the O’bidos lagoon (Portugal). *Cont Shelf Res* 26(8):917–942. doi:10.1016/j.csr.2006.02.011
- Parker BB (1991) The relative importance of the various nonlinear mechanisms in a wide range of tidal interactions (review). In: Parker BB (ed) *Tidal hydrodynamics*. John Wiley and Sons, New York, pp 237–268
- Prandle D (2003) Relationships between tidal dynamics and bathymetry in strongly convergent estuaries. *J Phys Oceanogr* 33(12):2738–2750
- Ralston DK, Geyer WR, Traykovski PA, Nidzicko NJ (2013) Effects of estuarine and fluvial processes on sediment transport over deltaic tidal flats. *Cont Shelf Res* 60:40–57
- Rao KK, Balasubramanian (1996) Distribution of foraminifera in the Cochin estuary. *J Mar Biol Ass India* 38(1&2):50–57
- Revichandran C, Srinivas K, Muraleedharan KR, Rafeeq M, Shivaprasad A, Vijayakumar K, Jayalakshmy KV (2011) Environmental set-up and tidal propagation in a tropical estuary with dual connection to the sea (SW Coast of India). *Environ Earth Sci*. doi:10.1007/s12665-011-1309-0
- Robins PE, Davies AG (2010) Morphological controls in sandy estuaries: the influence of tidal flats and bathymetry on sediment transport. *Ocean Dyn* 60:503–517. doi:10.1007/s10236-010-0268-4
- Shivaprasad A, Vinita J, Revichandran C, Manoj NT, Srinivas K, Reny PD, Ashwini R, Muraleedharan KR (2013a) Influence of saltwater barrage on tides, salinity and chlorophyll a in Cochin Estuary, India. *J Coast Res* 29(6):1382–1390
- Shivaprasad A, Vinita J, Revichandran C, Reny PD, Deepak MP, Muraleedharan KR, Naveen Kumar KR (2013b) Seasonal stratification and property distributions in a tropical estuary (Cochin estuary, west coast, India). *Hydrol Earth Syst Sci* 17:187–199. doi:10.5194/hess-17-187-2013
- Speer PE, Aubrey DG (1985) A study of non-linear tidal propagation in shallow inlet/estuarine systems. part II: theory. *Estuar Coast Shelf Sci* 21:207–224
- Srinivas K, Revichandran C, Maheswaran PA, Asharaf M, Murukesh N (2003a) Propagation of tides in the Cochin estuarine system, Southwest coast of India. *Indian J Mar Sci* 32:14–24

- Srinivas K, Revichandran C, Thottam TJ, Maheswaran PA, Asharaf M, Murukesh N (2003b) Currents in the Cochin estuarine system during March 2000 (Southwest coast of India). *Indian J Mar Sci* 32: 123–132
- Strikwerda M (2004) Cochin Estuary morphological modelling and coastal zone management PhD thesis. University of Delft, Germany
- Unnikrishnan AS, Shetye SR, Gouveia AD (1997) Tidal propagation in the Mandovi–Zuari Estuarine Network, West Coast of India: impact of freshwater influx. *Estuar Coast Shelf Sci* 45:737–744
- Vinita J, Shivaprasad A, Revichandran C, Manoj NT, Muraleedharan KR, Binzy J (2015) Salinity response to seasonal runoff in a complex estuarine system (Cochin Estuary, West Coast of India). *J Coast Res*. doi:10.2112/JCOASTRES-D-13-00038.1